Experimental Eye Research 201 (2020) 108326

Contents lists available at ScienceDirect

Experimental Eye Research

journal homepage: www.elsevier.com/locate/yexer

The human Descemet's membrane and lens capsule: Protein composition and biomechanical properties

Willi Halfter [a], Suzette Moes [b], Kathrin Halfter [c], Monica S. Schoenenberger [d], Christophe A. Monnier [a], Joanna Kalita [e], Daphne Asgeirsson [e], Tatjana Binggeli [a], Paul Jenoe [b], Hendrik P.N. Scholl [a,f,g], Paul Bernhard Henrich [a,h,*]

[a] Department of Ophthalmology, University of Basel, Switzerland
[b] Proteomics Core Facility, Biozentrum, University of Basel, Switzerland
[c] Munich Cancer Registry, Institute of Medical Informatics, Biometry and Epidemiology, Maximilian University Munich, Germany
[d] Swiss Nanoscience Institute, Nano Imaging Lab, University Basel, Switzerland
[e] Biozentrum and the Swiss Nanoscience Institute, University of Basel, Switzerland
[f] Institute of Molecular and Clinical Ophthalmology Basel (IOB), Switzerland
[g] Wilmer Eye Institute, Johns Hopkins University, Baltimore, MA, USA
[h] Università della Svizzera Italiana, Lugano, Switzerland

ARTICLE INFO

Keywords:
Basement membrane
Diabetes
Collagen IV
Laminin
Nidogens
Perlecan
Collagens
Proteomics
Mass spectrometry
Atomic force microscopy

ABSTRACT

The Descemet's membrane (DM) and the lens capsule (LC) are two ocular basement membranes (BMs) that are essential in maintaining stability and structure of the cornea and lens. In this study, we investigated the proteomes and biomechanical properties of these two materials to uncover common and unique properties. We also screened for possible protein changes during diabetes. LC-MS/MS was used to determine the proteomes of both BMs. Biomechanical measurements were conducted by atomic force microscopy (AFM) in force spectroscopy mode, and complemented with immunofluorescence microscopy. Proteome analysis showed that all six existing collagen IV chains represent 70% of all LC-protein, and are thus the dominant components of the LC. The DM on the other hand is predominantly composed of a single protein, TGF-induced protein, which accounted for around 50% of all DM-protein. Four collagen IV-family members in DM accounted for only 10% of the DM protein. Unlike the retinal vascular BMs, the LC and DM do not undergo significant changes in their protein compositions during diabetes. Nanomechanical measurements showed that the endothelial/epithelial sides of both BMs are stiffer than their respective stromal/anterior-chamber sides, and both endothelial and stromal sides of the DM were stiffer than the epithelial and anterior-chamber sides of the LC. Long-term diabetes did not change the stiffness of the DM and LC. In summary, our analyses show that the protein composition and biomechanical properties of the DM and LC are different, *i.e.*, the LC is softer than DM despite a significantly higher concentration of collagen IV family members. This finding is unexpected, as collagen IV members are presumed to be responsible for BM stiffness. Diabetes had no significant effect on the protein composition and the biomechanical properties of both the DM and LC.

1. Introduction

Basement membranes (BMs) are specialized extracellular matrices which outline muscle fibers, Schwann cells, and blood vessels (Yurchenco, 2011; Halfter et al., 2013a; Seikiguchi et al., 2018). Composed of approximately 30 different types of glycoproteins (Timpl and Brown, 1996; Ericson and Couchman 2000; Uechi et al., 2014), these thin yet surprisingly strong ECM sheets define the borders between

Abbreviations: BM, basement membrane; DM, Descemet's membrane; LC, Lens capsule; ECM, extracellular matrix; LC/MS, liquid chromatography/mass spectrometry; LN, laminin; AFM, Atomic Force Microscopy.

* Corresponding author. Department of Ophthalmology, University of Basel, Switzerland.
E-mail addresses: whalfter@pitt.edu (W. Halfter), suzette.moes@gmail.com (S. Moes), Halfter@ibe.med.uni-muenchen.de (K. Halfter), monica.schoenenberger@unibas.ch (M.S. Schoenenberger), christophe.a.monnier@gmail.com (C.A. Monnier), daphne.asgeirsson@gmail.com (D. Asgeirsson), t.binggeli@gmail.ch (T. Binggeli), p.jenoe@bluewin.ch (P. Jenoe), hendrik.scholl@usb.ch (H.P.N. Scholl), bernardohenrich@yahoo.com (P.B. Henrich).

https://doi.org/10.1016/j.exer.2020.108326
Received 13 June 2020; Received in revised form 18 October 2020; Accepted 20 October 2020
Available online 2 November 2020

epithelia and connective tissues, and are responsible for modulating many biological processes such as cell adhesion, differentiation, growth and wound healing. Their medical and biotechnological significance is therefore apparent and underlined by the severity of malfunctions such as early embryonic death, muscular dystrophy, skin blistering, cardio-vascular defects, eye, ear, and brain abnormalities (Miner et al., 1998; Costell et al., 1999; Smyth et al., 1999; Poeschl et al., 2004).

Two specific BM examples are the Descemet's membrane (DM) and the lens capsule (LC), both major constituents of the eye. With thicknesses of between 10 and 20 μm, these materials are among the most substantial BMs in the human body (Johnson et al., 1982; Danysh and Dunken, 2009; Zhang et al., 2018). Composed of different types of collagen IV and laminin, the DM is found in the posterior part of the cornea and represents a critical substrate for the non-replicating corneal endothelial cells, (Klintworth, 2009; Chen et al., 2017), whereas the collagen IV-rich LC forms the border between the lens and both the anterior and the vitreous chamber of the eye (Danysh and Dunken, 2009). Their high stiffness, expressed by their Young's moduli, is in the high kPa to low mPa range (Danielsen, 2004), which is several hundred-fold higher than the stiffness of cellular tissues which lie in the single digit kPa range (Janmey and McCuloch, 2007). The DM and LC, thereby, contribute prominently to proper eye configuration, shape and function, and disturbance of this equilibrium may lead to considerable pathology and loss of vision. The DM represents the stiffest layer of the cornea and is, thus, critical for corneal integrity, which in turn is paramount in protecting the eye from penetrating injury and in guaranteeing its refractive function. Pathophysiological alterations of the DM are expressed by a panoply of conditions, including corneal dystrophies (Zhang et al., 2019), Fuchs' endothelial dystrophy (Bruinsma et al., 2013; Zhang and Patel, 2015), bullous keratopathy (deOlivera et al., 2020), primary congenital glaucoma (de Olivera et al., 2020), keratoconus (Leukovitis et al., 2019) and systemic conditions such as Wilson's disease (Pandey and John, 2020). The LC, following constant changes in the shape of the lens during accommodation, has to be stiff to contain the lens fibers, but has to be elastic at the same time. It is noteworthy that, while the lens capsule reacts instantly in accommodation, the cornea takes minutes to regain its previous shape. Thus, it would be reasonable to assume that the components of the cornea, including the DM, exhibit a rigid stiffness, while the components of the LC allow for a higher instant elasticity. Apart from their role in accommodation, biomechanical properties are of critical importance during cataract surgery, where diseases, which involve the structure of the lens capsule (*e.g.* pseudoexfoliation syndrome) are linked to increased intraoperative capsular complications, namely anterior and posterior capsular rents (Droisum et al., 1998).

In a recent study by the authors, which relied upon the development of a simplified sample preparation method (Halfter et al., 2018) the protein composition of vascular BMs from the retina was investigated. By applying this sample preparation to the lens capsule (LC) and the Descemet's membrane (DM), we found that the composition of these BMs greatly differs, particularly in respect to their major protein components. Biomechanical measurements demonstrated, as expected, that the LC is considerably softer than the DM despite its much higher content of collagen IV (Cummings and Hudson, 2014).

This is the first comparative approach to analyze two morphologically very similar BMs side-by-side both with regards to their biochemical composition and biomechanical properties. While, not unexpectedly, the LC consists mainly of family members of the collage IV family, the dominant protein in DM is TGFBIp, the transforming growth factor-beta1-induced protein. It is a 70kD protein and not to be confused by the 17kD cytokine TGF beta 1. Mutations or absence of TGFBIp has been shown to be responsible for several forms of corneal dystrophy. A strong binding of TGFBIp to collagen IV has also been established (Hashimoto et al., 1997), indicating that the protein may be a natural component of other BMs as well. TGFBIp, however, is not listed as a common BM protein, and the importance of this protein in BM function has yet to be established. In a comparative proteomic study of BMs from different tissues, TGFBIp was one of the most consistent proteins in all BMs samples tested (Randless et al., 2017).

Further, preliminary analysis of DMs and LCs from diabetic donors demonstrated that changes in protein composition that we observed in retinal vascular BMs during diabetes (Halfter et al., 2018) do not occur in the LC and DM.

1.1. Experimental procedures

1.1.1. Preparation of basement membranes

Human donor eyes were obtained from CORE, the Center of Organ Recovery and Education (Pittsburgh, PA). The use of human eyes for this project was approved by the Internal Review Board of the University of Pittsburgh under the IRB protocol number # 0312072. Written consent for use of the bodies and organs, including eyes, for transplantation and research was given by the participants of this study during their lifetime, or by their next of kin. The time intervals between death and organ harvesting ranged between 2 and 7 h, with their delivery to the laboratory taking place the following day after screening for HIV and hepatitis. Lenses and corneas were dissected from donor eyes. The corneas were incubated in a 10 cm dish without shaking in 2% Triton X100 at room temperature overnight. Solid Deoxycholate was added to a final concentration of 1%. After 30 min incubation, the detergent-insoluble DMs were peeled from the inner surface of the cornea with fine forceps. The LCs were dissected from the lenses and incubated in Triton-X-100 and deoxycholate to remove the lens epithelia. Upon isolation, the BMs were stable and could be stored in PBS supplied with 0.01% sodium azide at 4 °C. Since BM protein composition is known to change with age (Candiello et al., 2010), BM samples from donors of similar age were analyzed.

1.1.2. SDS PAGE and western blots

For SDS PAGE, the BMs were solubilized by boiling in 8 M urea and 1x SDS sample buffer for 10 min. Samples were loaded onto 3.5–15% SDS gradient gels. For western blots, the proteins were transferred using a semi-dry blotting device (Biorad, Hercules, CA) to nitrocellulose (Trans-blot, Biorad). The blots were blocked with 1% skim milk. Antibodies to laminin (1:1000; Sigma, St. Louis, Mo) and collagen IV (1:2000; Rockland, Gilbertsville, PA) were used as primary antibodies. Alkaline-phosphatase-labeled secondary antibodies (Jacksin ImmunoResearch, West Grove, PA; 1:2000) were used, and the bands were visualized with NBT/BCIP.

For Western Blots, the same amount of protein (5 μg/lane) was loaded for each lane and each protein to be detected. Protein concentrations of the solubilized BM samples were determined as described by Minamide and Bamburg (1990).

1.1.3. Digestion of basement membranes and proteomic analysis

The BMs from both eye globes of one patient were spun at 10,000 rpm for 3 min, washed 3 times, and the pellet was taken up in 150 μL of PBS. 50 μL of collagenase (1000U/mL; type VII; Sigma) were added, and the sample incubated for 24 h at 37 °C. Next, the proteins were reduced with 10 mM DTT at 37 °C for 1 h and alkylated with 50 mM iodoacetamide for 15 min at room temperature. Protein digestion was performed by incubation of the sample with 1 μL trypsin (Sequencing grade, Promega) at 37 °C overnight. This digestion regime resulted in a complete solubilization of the BMs. The digest was desalted on a microspin column (The Nest Group, Southborough, MA, USA) according to the manufacturer's recommendations. Peptide absorbance was measured at 280 nm and peptide concentration was calculated according to Wisniewsky et al. (2009). Six micrograms were sufficient for the three technical LC-MS/MS replicate runs. LC-MS/MS analysis was performed on either an Orbitrap Elite or Orbitrap Classic (Thermo Scientific, Reinach, Switzerland) interfaced with an EASY-nLC 1000 pump connected to a C18 column (75 μm × 15 cm) packed with 2.4 μm Reprosil

particles (Ribitaille et al., 2013). For each analysis, equal peptide material (2 μg) was injected in triplicates onto the capillary column. Chromatography and mass spectrometric parameters corresponded to methods described in (Robitaille et al., 2013).

The LC/MS/MS data were searched against the human databank from SwissProt. The databank was updated monthly. The Mascot and Sequest HT search engines were run *via* Proteome Discoverer 1.4 (Thermo Scientific). Search parameters were set to carbamidomethylated cysteines as fixed modification, whereas oxidized methionines, and protein N-terminal acetylation were selected as variable modifications. Peptides that had a false discovery rate below or equal to 1% were accepted. For relative protein quantification, the ion intensity for the identified peptides was integrated as area under the curve from which the total intensity for a given protein was calculated using Proteome Discoverer 1.4, a standard procedure for label-free protein quantification in mass spectrometry (Nelison et al., 2011). Each data set was analyzed in three technical replicates.

We also compared the proteomes of an LC sample from Pittsburgh with a lens capsule sample obtained from cataract surgery in Basel, Switzerland. No major differences in the proteomes of these two samples were detected. The data also showed that the lens capsule sample from a single cataract surgery was sufficient for the LC-MS/MS analysis (data not shown).

1.1.4. Immunohistochemistry

DM and LC segments were spread onto Superfrost-plus slides (Fisher Scientific, Waltham MA) coated with 5 μg/mL poly-lysine (Sigma, St. Louis, MO). For firm attachment of the BM sheets, the slides were centrifuged at 1000 rpm for 5 min. The whole mounts were washed twice with 1% BSA, 0.01% Triton-X-100 and stained with polyclonal antisera to collagen IV (Rockland, Gilbertsville, PA), laminin (Sigma, St. Louis, Mo), or a mouse monoclonal antibody to the 7S-domain of collagen IV α3 (Mab J3-2; kindly provided by Dr. Nirmala Sundarraj (Sundarraj and Wilson 1982). The specified IgM antibody is also available from Sigma Aldrich (SAB4200500). A polyclonal rabbit antibody to TGFBIp was from Abcam (ab 189778). Secondary antibodies were Cy3 or Alexa-Fluor 488-labeled goat ant-rabbit, goat anti-mouse, or mu-chain-specific goat anti-mouse antibodies (Jackson ImmunoResearch, West Grove, PA; and Life Technologies, Carlsbad CA). Micrographs were taken with an Olympus Flow-view confocal microscope. For detecting proteins in whole mounts, the BMs were stained while in suspension and were then immobilized onto slides. The confocal images of the whole mounts were taken at 20 levels through the entire BMs und the stacks of images were collapsed into a single image. Cross-sections of the stacks from the confocal images were generated by the microscope software.

1.1.5. Atomic force microscopy (AFM)

DM and LC sheets were spread onto either Superfrost-plus glass slides (Fisher Scientific, US) or 2 cm tissue cultures dishes (TPP AG, Switzerland) and firmly mounted onto the substrates by centrifugation as described above. For the LC, only segments of the frontal part of the lens were probed. The measurements were performed using a JPK NanoWizard 4 (Bruker Nano GmbH, Berlin, Germany). Standard silicon nitride triangular cantilevers and integrated sharp silicon nitride pyramidal tips with nominal spring constants of 0.07 N/m and radii of around 10 nm were used, and their spring constants were determined in PBS prior to every experiment by using the Sader method (Sader et al., 1999). Force spectroscopy was performed with a load of 800 pN, with indentation depths ranging of between 50 and 400 nm. The indentation speed of the loading and unloading path was set to 2 μm/s. Three samples of each BM were probed, and force-displacement curves were recorded on both endothelial/epithelial and stromal/anterior-chamber sides at three different locations, each over a scanning area of 10 × 10 μm. From these data, the elastic moduli were calculated with the JPK Data Processing software by using the Oliver-Pharr model (Oliver and Pharr, 1992).

2. Results

2.1. Human Descemet's membrane (DM) and Lens capsule (LC)

We isolated both the DMs and LCs from each three pairs of donor eyes from non-diabetic and diabetic donors (biological repeats, n = 3 each). Table 1 and Supplementary Table S7 list age, gender, and medical history of the donors, including their cause of death. BM isolation involved incubating corneas in Triton-X-100 and deoxycholate, and subsequently peeling the DM from the de-cellularized corneas. The lens capsules (LCs) were dissected from the isolated human lenses with forceps. They were then treated with detergent to remove the lens epithelial cells. Both BMs appeared under a dissecting microscope and dark-field illumination as transparent sheets that were always curled up (Fig. 1A). As shown previously (Halfter et al., 2013b, 2013b, 2015; 2013b), the outer surfaces of the curled BMs represented the endothelial/epithelial side facing the corneal endothelium or the lens epithelium, whereas the inner curved surface faced the stromal/anterior-chamber side, *i.e.*, the corneal stroma or the anterior eye chamber (Fig. 1B–E). Light microscopy (Fig. 1), transmission and scanning electron microscopy images (Halfter et al., 2013a, 2013b, 2015) confirmed that the isolated BMs were clean, transparent ECM sheets that were not contaminated with nuclear or cellular debris. Additional evidence for the absence of cellular components came from whole mounts stained with CytoxGreen, a generic nuclear dye, which confirmed that both BMs were not contaminated with any intact or fragmented nuclei (Supplementary Fig. 1). Likewise, the proteomics data confirmed the very low abundance of nuclear, cytosolic or cytoskeletal proteins in the proteome data lists (Supplemental tables S1–S6 and S8–S13, Sheets 1).

SDS-PAGE analysis of the BMs showed different protein banding patterns for the DM and LC (Fig. 2). Coomassie staining (Fig. 2) revealed that the protein yield from a single lens capsule was much greater than that from a single DM. Second, the dominant LC proteins ranged between 400 and 150 kD, whereas the most dominant band of the DM had a molecular weight of around 70 kD, the expected molecular weight of TGF beta1-induced protein (TGFBIp, the dominant protein of the DM, see below). First, Western Blots (Fig. 2) using DM and LC samples normalized for identical protein concentration revealed that the collagen IV concentration in the LC samples was much greater than in the DM samples. Second, laminin γ1 was present in similar amounts in both the LC and DM, and, third, collagen IV showed a higher abundance than laminin in both BMs.

LC and DM samples were further analyzed by LC-MS/MS for an unbiased and comprehensive identification of the protein differences between both BMs, and the identified proteins were subsequently compared to each other.

2.2. The human DM proteome

2.2.1. Sample processing and Identification of DM proteins

For the LC-MS/MS analysis of the BMs, samples were digested with collagenase, followed by a second round of trypsin digestion. The combined enzyme treatments led to a complete solubilization of the BMs. This was verified in pioneering experiments by the absence of any insoluble material after centrifugation and microscopic inspection of the BM digests. The total peptide yield for DM samples from the three pairs of eyes ranged between 99 and 220 μg (mean: 154 ± 61%, n = 3; Table 1). Using a stringent 1% peptide false discovery rate cutoff, we identified between 61 and 93 proteins for the three DM samples (mean: 74 ± 17%, n = 3; Table 1; Supplementary Tables S1–3, Sheets 1). Between 36 and 58 of the identified DM proteins were ECM constituents (mean: 44 ± 12%; Table 1, Supplemental Tables S1–3, Sheets 2), accounting for 58–62% of the identified proteins (mean: 60 ± 2%; n = 3;

Table 1
Samples used for the MS analysis of on-diabetic DMs and LCs. The table lists age of the donors, their gender, cause of death, the peptide yields after collagenase and trypsin digestion (in μg), the total number of detected proteins, the number of ECM proteins and the percentage of ECM proteins relative to the total number of proteins. The data for the LC samples are in red. SIGSWS: self-inflicted gunshot wound; MI: myocardial infarction; AAA: abdominal aortic aneurism. The data for the LCs are in red. DM and LC samples came each from the same donors.

Age, gender, DM or LC	Cause of death	Peptides (μg)	Proteins (#)	ECM proteins (#)	ECM (%)
64y m DM	MI	143	93	58	62
64y m LC	MI	530	52	38	73
65y m DM	AAA+MI	99	61	36	59
65y m LC	AAA+MI	211	109	47	43
47y m DM	SIGSW	220	67	39	58
47y m LC	SIGSW	118	41	26	63
Mean DM (μg)		**154**	**74**	**44**	**60**
Std. dev. DM (%)		61	17	12	2
Mean LC (μg)		**286**	**67**	**37**	**60**
Std. dev. LC (%)		216	37	11	15

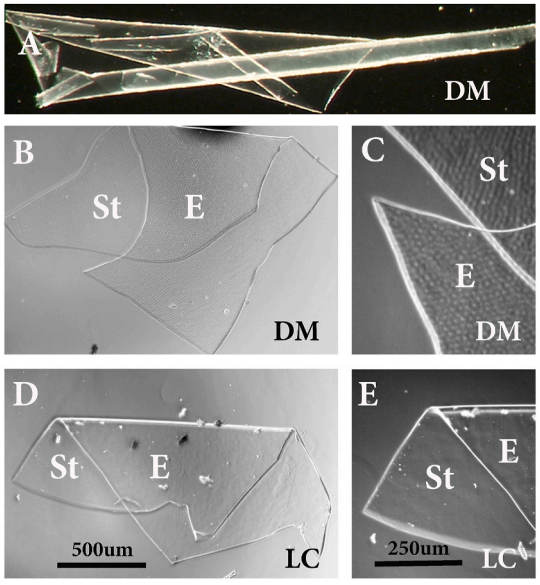

Fig. 1. Free-floating DMs (A), flat-mounted DMs (B, C) and LCs (D, E) from human eyes. The Both BMs were always curled (A). They were flat-mounted on slides in a folded configuration, whereby the epithelial (Endothelial/epithelial; E) and the stromal/anterior-chamber side (St/AC) were exposed side-by-side. B, D: low power, C, E: higher power. Scale Bars: B, D: 500 μm; C, E: 250 μm.

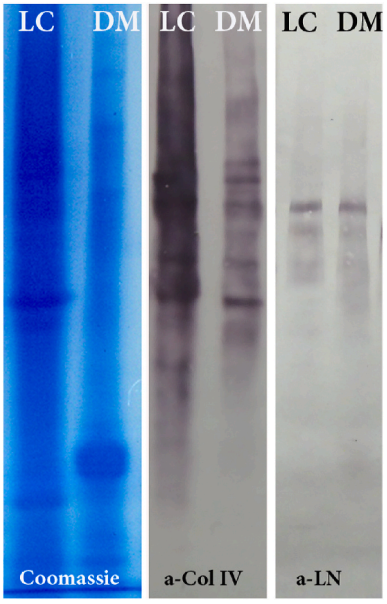

Fig. 2. SDS-PAGE and Western Blots showing the LC and DM protein banding after Coomassie (Coom) staining. A similar aliquot of the urea extract of one DM and one LC showed more protein for the LC than for the DM. The dominant band for the LC ranged between 400 and 150 kD. The dominant Coomassie-stained protein band for the DM was at 70 kD. For the Western Blots, the protein loaded onto the gel slots was normalized to 5 μg protein per lane. Anti-laminin (aLN) labeling showed that the laminins were present in the LC and DM in similar concentrations. Anti-collagen IV labeling (aColl4) showed the high abundance of collagen IV chains in the LC, with much less collagen IV in the DM. Further, there was more collagen IV than laminin in both samples.

Table 1; Supplementary Tables S1–3, Sheets 2).

2.2.2. Relative concentrations of DM proteins

To determine the relative concentrations of the individual proteins in each of the DM samples, the ion intensity for all the identified peptides of a protein was integrated as area under the curves. The abundance of a given protein in the entire sample was expressed as percentage relative to the total protein of each sample that was set to 100%. The pie charts on Supplementary Tables S1–3, Sheets 1 graphically illustrate the relative abundance of the individual proteins per sample. The 39 to 58 ECM proteins accounted for between 67 and 82% of total protein in the three DM samples (mean: 76 ± 8, Table 2, ECM column). The non-ECM proteins of the DM samples were cytoskeletal constituents and cytoplasmic proteins. A consistent non-ECM protein was clusterin, a chaperon protein that also exists as a secreted 68 kD protein (Wilson and Easterbrook-Smith, 2000; Wyatt et al., 2009). It accounted between 0.8 and 5.3% of the total proteome (mean: 3.3 ± 2.3%; n = 3; Supplementary Tables S1–3, Sheets 1). Nuclear proteins, such as histones were not found in any of the DM samples (Supplementary Tables S1–3, Sheets 1).

In the next step of proteome data processing, all non-ECM proteins were subtracted from the total proteome data sets for each sample, leading to a list of ECM proteins for each DM sample (Supplementary Tables S1–3, Sheets 2). The abundance of identified individual ECM protein was then calculated as percentage relative to 100% of the ECM

Table 2
Proteins as detected in DM and LC samples. Column One identified the donors according to their age. Column Two lists the total number of proteins that account for 100% of the total protein. Columns Three to Seven lists the number of total ECM proteins, the percentage of ECM proteins among all proteins detected, the percentage of TGFBIp, and the percentage of collagen IV-, and laminin family members relative to the total protein content of the samples. nd: not detectable. The data for the LC samples are in red.

Age, gender DM or LC	Total # of proteins (=100%)	ECM (#)	ECM (%)	TGFBIp (%)	Coll 4 α1, 2; α3-6 (%)	LN α5, β1, γ1 (%)
64y m DM	93	58	80	41	12%	3.5%
64y m LC	52	38	79	0.03	54%	4.8%
65y m DM	61	36	82	58	6.5%	2%
65y m LC	109	47	82	0.05	53%	3.7%
47y m DM	67	39	67	34	7.9%	2.2%
47y m LC	41	26	92	0.05	72%	3.5%
Mean % (n=3) DM			**76%**	**44%**	**8.7%**	**2.5%**
Std. dev. DM			8%	12%	2.5%	0.7%
Mean % (n=3) LC			**84%**	**0.04%**	**59%**	**4.0%**
Std. dev. LC			7%	0.01%	10%	0.6%

proteome per sample, and is listed and graphically illustrated in the Pie Charts on Supplemental Tables S1–3, Sheets 2.

The lists of identified ECM proteins of all three samples of the DM samples were then compared, and proteins encountered in at least two of the three DM samples were selected as reliable DM proteins (Table 3). Forty-two ECM proteins were shared at least twice in the three DM samples (Table 3, Column 2, N at least 2). The list and relative abundance of proteins found in DMs included four of the six existing collagen IV peptide chains, with the main collagen family members of α3, 4, 5 (12% of the total DM proteome). It also included collagen VI α1, α2 and α3 (1.9%), three laminin chains (α5, β1, γ1; 3%), nidogen I (0.4%) and the proteoglycans perlecan (1.3%), agrin (0.5%) and keratokan (0.9%). Additional protein components were vitronectin (2%), collagen XVIII (0.25%) and fibulin 1 and 5 (3.8%). The most prominent DM protein, however, was TGF-induced protein (TGFBIp) with a mean of 54% of the total DM proteome.

2.3. The human LC proteome

2.3.1. Processing and identification of proteins of the LC samples

The LC samples were processed in the same way as described above. The peptide yield for each of the three LC samples was between 118 and 530 μg of total peptide (mean: 286 ± 216 μg, n = 3; Table 1). For the LC samples, we found a total of between 41 and 109 proteins (mean: 67 ± 37, n = 3, Table 1; Supplementary Tables S4–6, Sheets 1), between 26 and 47 of which were ECM proteins (mean: 37 ± 11; Supplementary Tables S4–6, Sheets 2). This equaled between 43 and 75% of the total identified proteins (mean: 60 ± 15%, n = 3; Table 1; Supplementary Tables S4–6, Sheets 2).

2.3.2. Relative concentration of LC proteins

The 26 to 47 ECM proteins from the LC samples accounted for 79–92% of the total protein within the samples (mean: 84 ± 7%, Table 2, column ECM, Supplementary Tables S4–6). The most prominent proteins among the ECM proteome were members of the collagen IV family, α1 and α2 chains being the most prominent ones with a mean of 44%, n = 3 (Table 3). The remaining α-chains 3, 4, 5 and 6 had a mean of 29% (Table 3). The main consistent non-ECM protein of the LC was clusterin (mean: 4.1 ± 3.2%; Supplementary Table S2, Sheet 1). No nuclear proteins were detected in any LC sample (Supplementary Tables S4–6, Sheets 1). A list of reliable LC proteins, the ECM components found in at least two of the LC samples were selected (Table 3).

Twice-shared ECM proteins of the three LC samples numbered in total thirty-two. It included all six collagen IV family members. Dominant collagen IV family members were the α1 and α2 chains followed by the α3, 5 and 6-chains. The collagen IV members accounted in total for 73% of the total ECM proteome of the LC. The laminins α5, β2 and γ1 accounted for 4% of the ECM proteome and perlecan, the dominant proteoglycan accounted for 8% of the ECM proteome. Metalloproteinase 3 was with 6.6% also a prominent component of the LC proteome.

2.4. Comparison of human DM and LC proteomes

In a first approach we illustrated the differences in the protein composition between LC and DM proteomes, by comparing the DM and LC proteomes of a single, but representative sample. Pie charts from DM and LC samples of the same 47-year old donor demonstrated the abundance of six α1-to α6 collagen IV chains in the LC, which accounted for over 75% of the entire ECM proteome of this sample (Fig. 3). The most abundant protein in DM was TGF-beta-induced protein (TGFBIp) with over 50% of the DM proteome. The most abundant collagen IV trimer in the DM had a chain composition of α3, 4 and 5, which accounted for less than 12% of the ECM proteome of the DM. These differences were also observed with the other remaining DM and LC samples, as shown in the bar graphs in Fig. 4A and B.

The bar graphs of Fig. 4A and B shows in detail the ECM proteins detected in all nom-diabetic DMs and LCs side-by-side. The most prominent proteins are shown in Fig. 4A, the less abundant at a lower scale in Fig. 4B. Collagen IV α1 and α2 family members were only detected in the LC, while TGFBIp, was most prominent in the DM (Fig. 4A). Among the prominent proteins, collagen VI family members and collagen XII were only detected in the DM, while laminin β2 and nidogen 2 were only detected in the LC. A major difference was also the

Table 3
ECM proteomes of the DM and the LC. The ECM proteins that were detected in two of the three DM or two of the three LC samples are listed. Proteins shaded in green were most prominent, whereas the proteins listed in yellow were less prominent. Column One lists the number of cases, in which the proteins were detected in the three samples, column Two the mean relative abundance in % relative to the 100% DM or LC proteome. Column Three: lists the standard deviations. (Incidence rates: green = very high, red: high; pink = intermediate, yellow = low).

	DM			LC		
Description	N	Mean	StDev	N	Mean	StDev
Coll IV a1				3	25.35	8.11
Coll IV a2				3	18.58	6.52
Coll IV a3	3	4.4	0.9	3	12.23	2.47
Coll IV a4	3	2.8	0.6	3	1.57	0.95
Coll IV a5	3	3.10	1.2	2	9.07	11.52
Coll IV a6	2	0.8	0.7	3	6.25	4.54
CollVI a1	3	0.48	0.34			
Coll VI a2	2	0.33	0.08			
Coll VI a3	3	1.07	1.03			
Coll XII a1	3	0.48	0.19			
Coll XVIII	2	0.25	0.21	3	0.24	0.06
LN a5	3	1.10	0.45	3	1.43	0.04
LN b1	3	0.82	0.31	3	0.16	0.06
LN b2				3	1.45	0.29
LN g1	3	0.82	0.37	3	1.18	0.31
Nidogen-1	3	0.43	0.16	3	0.63	0.33
Nidogen-2				3	0.24	0.06
Perlecan	3	1.33	0.70	3	7.95	4.36
Agrin	3	0.51	0.28	3	0.29	0.16
Keratocan	3	0.88	0.43			
Prolargin				2	0.13	0.01
TGFBIp	3	54.57	15.73	3	0.05	0.01
TINAG				3	2.62	1.23
Vitronectin	3	1.97	0.38	3	1.66	0.96
Fibrillin-1				3	2.28	2.12
Fibulin-1	3	1.57	0.34			
Fibulin-5	3	2.28	0.72			

	DM			LC		
Description	N	Mean	StDev	N	Mean	StDev
SPARC-like protein 1	3	0.15	0.04			
Thrombosp.1	2	0.19	0.13			
Thrombosp.4	3	3.90	0.57			
Olfactomed.	3	0.20	0.04			
Opticin				2	0.40	0.07
Papilin				3	0.16	0.07
Microfib-ass. Prot				3	0.46	0.07
EMILIN-3				2	0.07	0.01
His-rich Prot.	3	0.19	0.08			
EGF-Fibulin	2	0.30	0.07			
EMILIN-1	3	0.54	0.32			
AMBP	2	0.70	0.42			
Apo E	3	0.16	0.04	3	0.20	0.19
C-Type lectin dom	3	2.80	1.49	2	0.13	0.08
ADAMTS-I-Prot				3	0.15	0.03
C3	2	0.11	0.16			
C4-A	2	0.35	0.25			
Myocilin	3	0.94	0.85			
C8	2	0.08	0.11			
CH	3	0.09	0.09			
C9	3	0.40	0.28			
Metallo Prot. Inhib.	1	0.23	NA	3	6.62	5.94
Serine protease 56				2	0.07	0.04
Serine protease HTRA1	3	0.52	0.26	2	0.04	0.01
Carbohydr. Sulfotransf.	2	0.22	0.31	2	0.29	0.04
Carbohydr. Sulfotransf.	2	0.05	0.01	2	0.17	0.04
Extrac. Superoxide Dismutase	2	1.24	1.60			
Noggin	2	0.08	0.02			

high abundance of perlecan in the LC relative to the DM. Minor proteins were shown in a separate bar graph (Fig. 4B) to demonstrate their existence with a lower scale percentage. Again, several prominent proteins were only detected in DM, while others were proteins present in only LCs. For example, LC-specific minor proteins were TINAG and fibrillin-1.

2.5. DM proteomes from diabetic and non-diabetic donors

Previous studies have shown that long-term diabetes leads to changes in the proteome of the retinal vascular BMs (To et al., 2013; Halfter et al., 2018). The list of proteins in vascular BMs from diabetic donors was consistently longer in diabetic versus non-diabetic BMs, and it revealed of seven proteins that were detected in diabetic but not in

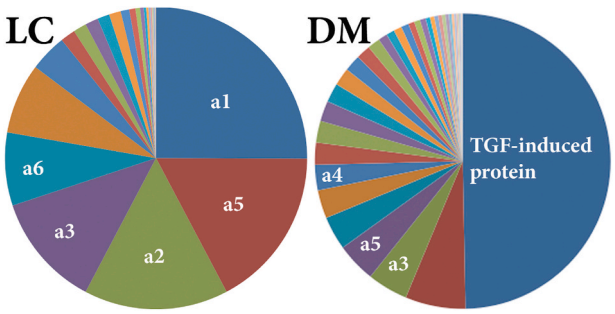

Fig. 3. Representative pie charts showing the relative protein component concentrations of the LC and DM from a single 47-year old human donor. The α1 to α6 collagen IVs accounted for over 75% of the ECM proteome of the LC, but only for less than 15% of the DM. The dominant protein in DM was the TGF-beta-induced protein (TGFBIp).

non-diabetic donors. Further, we found statistically significant increased levels of several complement proteins, and norrin, a growth factor necessary for retinal vascularization. In an exploratory approach, we investigated whether we would find similar differences in the LC and the DMs proteomes from diabetic and non-diabetic patients. We processed and analyzed each a diabetic and a non-diabetic DM sample in parallel to avoid possible variations in the experimental processing. The list of diabetic donors, the duration of their diabetic condition, and the cause of death are listed in the Supplementary Table S7.

The peptide yield for three DM samples from diabetic donors was between 44 and 205 μg (mean: 109 ± 84 μg). We identified between 68 and 79 proteins for the three diabetic DM samples (mean: 75 ± 6, n = 3; Supplementary Tables S8–10, Sheets 1). Between 41 and 45 of the identified DM proteins were ECM constituents (mean: 42 ± 2), accounting for 52–60% of all identified proteins (mean: 56 ± 4%; n = 3; Supplementary Tables S8–10, sheets 2). We then determined the relative concentration of each of the proteins as shown above and obtained a list of reliable DM proteins from the diabetic donors.

The relative quantities of the identified proteins from the diabetic and non-diabetic DM samples were then contrasted as shown in Supplementary Table S9. The table further shows that forty-one proteins of the combined forty-six listed proteins were identified in the non-diabetic DM samples, and forty-two of the forty-six total listed proteins were present in the list of the diabetic DM samples. Thus, there was an almost complete overlap in the proteomes of the DMs from diabetic and non-diabetic donors.

The few differences that we detected were not statistically significant; The number of proteins in the combined proteome from non-diabetic samples was slightly longer than that from the diabetic donors. The bar graph comparing the diabetic and non-diabetic proteomes is shown in Fig. 5. The graph compares the mean abundances of proteins present across all diabetic and all three non-diabetic donor samples.

More abundant in diabetic than non-diabetic samples were serum protease HTRA1 (1.1 *versus* 0.52%), and extracellular superoxide dismutase (0.05 *versus* 1.2%). The relative abundance of collagen IV members combined was slightly lower than in the non-diabetic DM samples (Fig. 5). Myocillin was another protein that was more abundant in non-diabetic vs diabetic samples (0.5 *versus* 0,9%).

2.6. LCs proteomes from diabetic and non-diabetic donors

We also determined the LC proteomes from diabetic donors and compared them to non-diabetic counterparts. The peptide yield for the LC samples from diabetic donors was between 52 and 288 μg (mean: 169 ± 118 μg). We identified between 35 and 101 proteins for the three diabetic LC samples (mean: 63 ± 34, n = 3; Supplementary Table 3; S12-14, Sheets 1). Between 23 and 40 of the identified DM proteins were ECM constituents (mean: 30 ± 9), accounting for 40–66% of the identified proteins (mean: 53 ± 13%; n = 3; Supplementary Table 3; S12-14, Sheets 2). We then determined the relative concentration of each of the

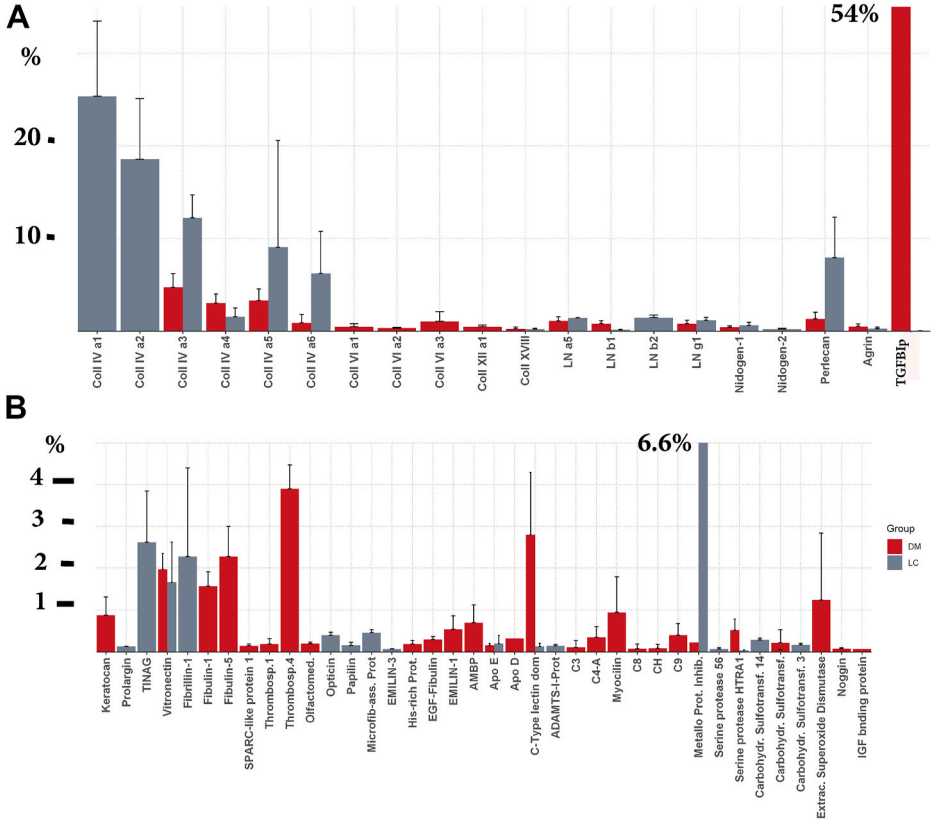

Fig. 4. A: Graphic representation showing the relative abundance of dominant ECM proteins in DMs (red bars) and LCs (grey bars) in percent relative to the entire ECM proteomes. Listed are the collagen IV- and laminin-family members, nidogen 1 and 2 and the proteoglycans perlecan and agrin. Listed as well is TGFBIp, the TGF-induced protein, which is the most prominent protein in the DM proteome. The means from three DM and LC analyses with standard deviations are shown. Col: collagen-family members; LN: laminin-family members. TGFBIp: TGF-beta1-induced protein. Fat bars indicate that these proteins were only detected in one of the two BMs. B: Graphic representation showing the relative abundance of less dominant ECM proteins in DMs (red bars) and LC donors (grey bars), in percent relative to the entire ECM proteome. The means from three DM and LC analyses with standard deviations are shown. C: complement. Fat bars indicate that these proteins were only detected in one of the two BMs. Note the different scale bar as compared to Fig. 4A. (For interpretation of the references to colour in this figure legend, the reader is referred to the Web version of this article.)

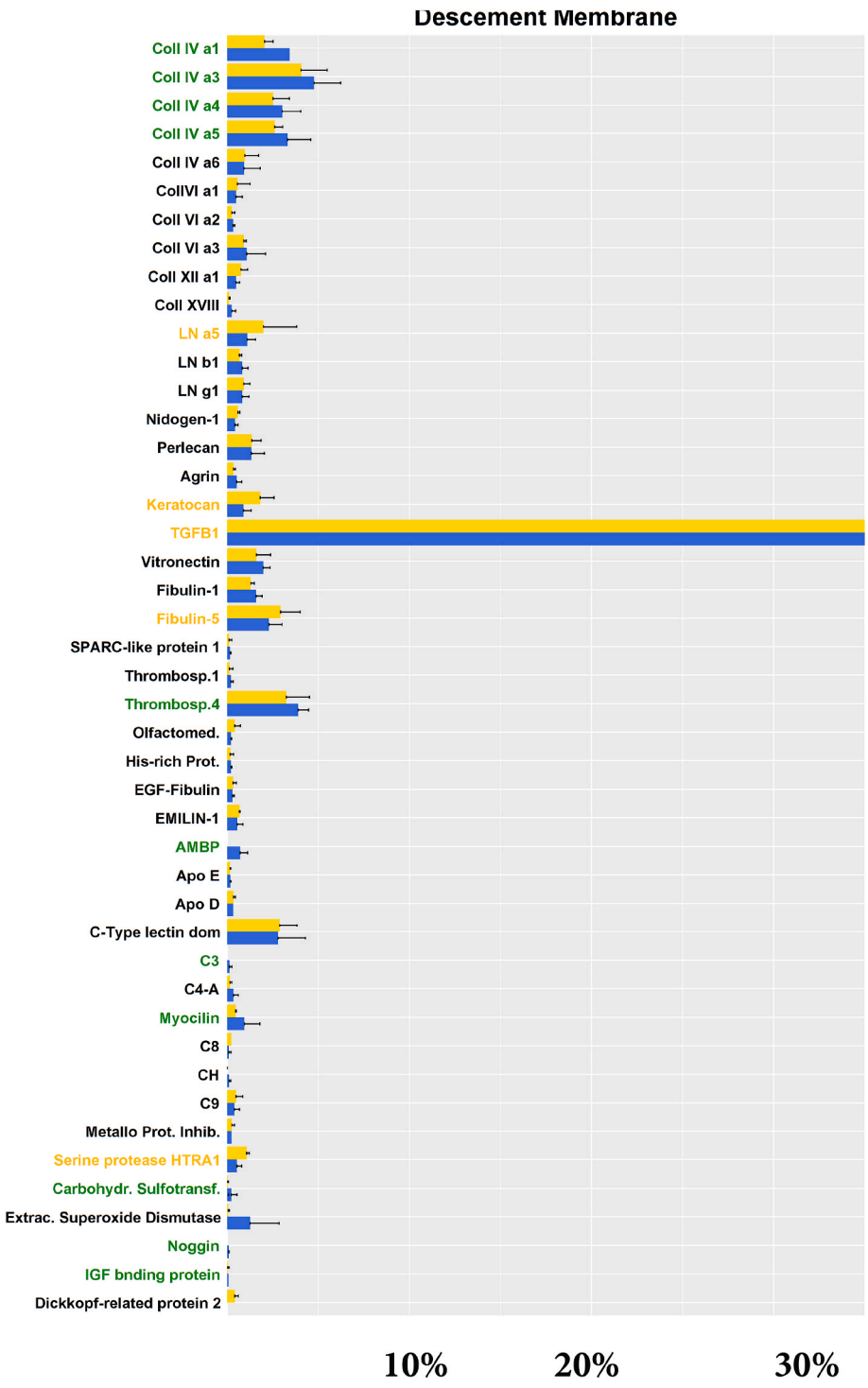

Fig. 5. Graphic representation showing the relative abundance of ECM proteins in DMs from diabetic (yellow bars) and non-diabetic donors (blue bars) in percent, relative to the entire ECM proteome set to 100%. The means from three diabetic and three non-diabetic DM analyses with standard deviation are shown. The proteins that are more abundant in diabetic as compared to non-diabetic BMs are labeled in yellow, the proteins less abundant in green. Col: collagen-family members; LN: laminin-family members, C: complement. (For interpretation of the references to colour in this figure legend, the reader is referred to the Web version of this article.)

proteins as shown above and obtained a list of reliable LC proteins from the diabetic donors.

The relative quantities of the identified proteins from the diabetic and non-diabetic LC samples were then contrasted as shown in Fig. 6. There was an almost complete overlap in the LC proteomes from diabetic and non-diabetic donors. As with the DM, the list of proteins from diabetic donors was slightly shorter than that from the non-diabetic donors. The collagen IV family members appeared to be more abundant in the diabetic samples, but the difference was not statistically significant. Perlecan and metallo-proteinase inhibitor 3 were more abundant in non-diabetic samples, but, again, the differences were not statistically significant.

In summary, the proteomes of DMs and LCs from diabetic and non-diabetic donors are similar, and they do not show the unique protein expressions that we found with diabetic vascular BMs. The data from the proteome analysis, however, confirmed and solidified the proteome data that we obtained from the analysis of BMs of non-diabetic donors.

2.7. Localization of DM and LC proteins

We reverted to immunohistochemistry to assess the distribution of several proteins in the DM and LC. Whereas stained sections showed the

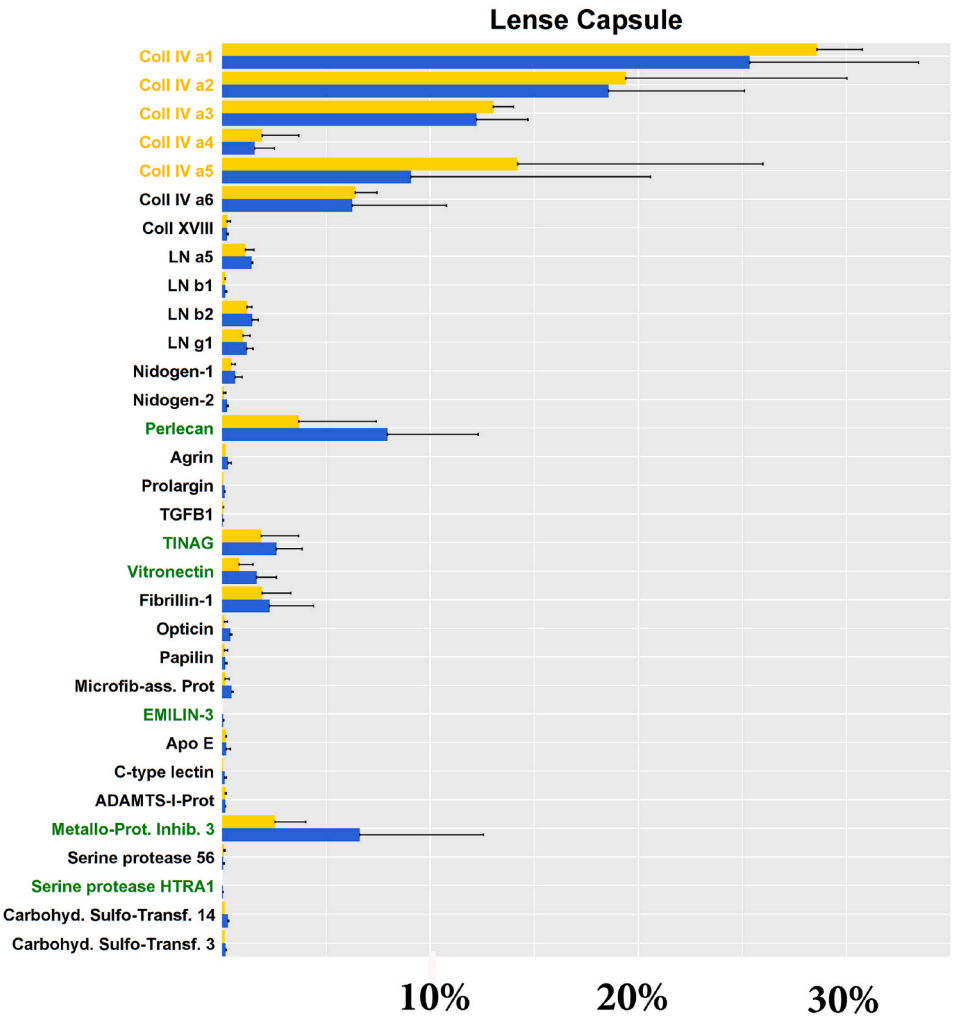

Fig. 6. Graphic representation showing the relative abundance of ECM proteins in LCs from diabetic (yellow bars) and non-diabetic donors (blue bars) in percent, relative to the entire ECM proteome set to 100%. The means from three diabetic and three non-diabetic BM analyses with standard deviation are shown. The proteins that are more abundant in diabetic as compared to non-diabetic BMs are labeled in yellow, the proteins less abundant in green. (For interpretation of the references to colour in this figure legend, the reader is referred to the Web version of this article.)

vertical distribution of proteins (Fig. 7A and B), BM whole mounts allowed an overview of a larger segment (Fig. 7 C). Polyclonal antisera to laminin and collagen IV stained both BMs, and they were abundantly present. As shown previously (Kobasova et al., 2007; Halfter et al., 2013b; Reyes-Lua et al., 2016), the laminin labeling was localized to the former endothelial sides of the DM (Fig. 7A) and to the epithelial side of the LC (Fig. 7B), while a monoclonal antibody to the 7S-domain of collagen IV a3 labeled the stromal side of the DM and the anterior-chamber side of the LC (Fig. 7A and B). In view of the surprising abundance of TGFBIp in the DM, we stained DM whole mounts with an antibody to this protein. Subsequent fluorescence imaging by confocal microscopy showed that the protein is uniformly polarized to the

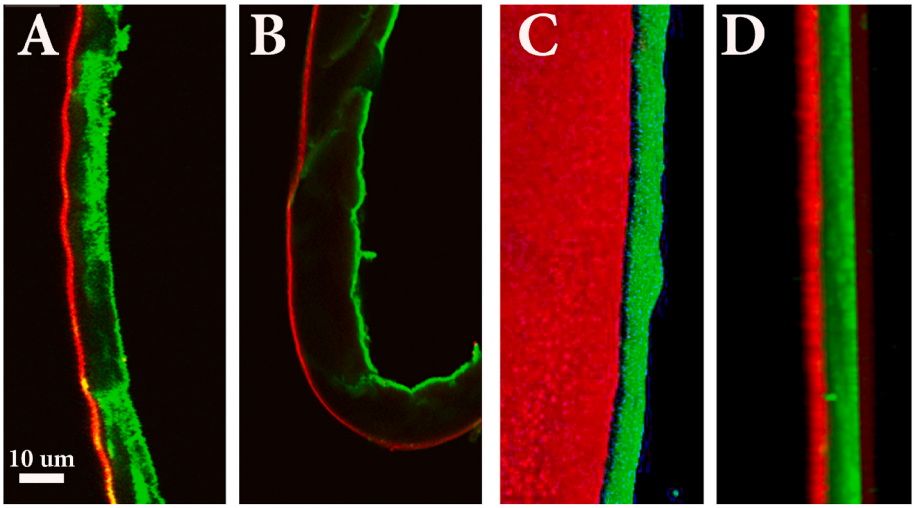

Fig. 7. Staining of DM (A) and LC crossections (B). In both cases, laminin was localized on the endothelial side of the DM (A) and the epithelial side of the LC B). The Collagen IV α3-staining labeled the stromal (A) and the anterior chamber sides (B). A confocal image of a DM whole mount stained for TGF-induced protein (red) and collagen IV a3 (green) is shown in (C). The stack of 20 images through the DM had been collapsed. The endothelial side is up. TGFBIp is present over the entire endothelial surface of the DM (C). The green edge stained for collagen IV is due to the wedge-shaped rim of the DM that is exposing a small segment of the stromal side of the BM. The crossectional image of the whole mount is shown in (D). The endothelial side is facing left. Both images show that TGFBIp is localized on the endothelial side of the DM, while collagen IV is localized on the stromal side of the DM. Bar: 10 μm. (For interpretation of the references to colour in this figure legend, the reader is referred to the Web version of this article.)

endothelial sides of the DM (Fig. 7C). A cross-sectional image was created by collapsing all confocal images through the entire whole mounts. This confirmed the endothelial localization of TGFBIp and exhibited collagen IV labeling at the stromal side (Fig. 7D). Acid-treatment of the sections or the whole mounts to unmask possibly hidden antigenic sites did not change these side-specific staining patterns.

2.8. Biomechanical testing by atomic force microscopy (AFM)

BM whole mounts were probed for stiffness by atomic force microscopy (AFM) to compare their biomechanical properties and to investigate whether they related to differences in protein composition. The light micrograph in Fig. 8A shows a folded DM sample with a superimposed AFM tip and illustrates a representative experimental setup.

We first probed the stiffness of each of the BMs. As data of the previously tested BMs suggested, the stromal and epithelial sides are biomechanically different (Halfter et al., 2013a). Thus, we probed both sides of the BMs side-by-side (Table 4; and Fig. 8C and D). These measurements showed that the endothelial/epithelial sides were stiffer than their respective stromal/anterior-chamber sides. The side-specific stiffness applied for both DM and LC samples (Table 4; Fig. 8).

In a second data processing approach, we compared the stiffness of the DM with the stiffness of the LC, which showed that the DM is stiffer than the LC. This applied to both the endothelial/epithelial as well as to the stromal/anterior-chamber sides (Table 4 and Fig. 8).

Finally, we compared the stiffness values of diabetic and non-diabetic DMs and LCs. For this, samples from three non-diabetic human retinas and three specimens from diabetic human donors were probed, and stiffness data were generated and confirmed in three different data collections. For each BM sample, we compared the stiffness from the endothelial/epithelial and from the stroma/anterior-chamber sides.

The mean stiffness of the endothelial sides of the DM was 600 kPa in non-diabetic samples versus 900 kPa in diabetic samples (Fig. 9B). This difference was not statistically significant. The same applied for the stromal stiffness, with 200 kPa for the samples from non-diabetic donors and 300 kPa (n = 5) for the samples from diabetic donors (Fig. 9B).

For the epithelial sides of the LC, we measured a mean stiffness of 200 kPa for non-diabetic donors and 180 kPa for diabetic ones (Fig. 9C).

Table 4
Shows the AFM-based stiffness data from three different DM and LC flat mounts. Data are given as means with standard deviations. Results show that the endothelial/epithelial sides of DM and LC are stiffer than their respective stromal/anterior-chamber sides.

	Endothelial/Epithelial (kPa)	Stromal/anterior chamber (kPa)
DM	644.2 ± 171.6	221.8 ± 92.7
LC	217.0 ± 106.8	32.9 ± 12.0

For the anterior-chamber sides of the LCs, a mean stiffness for non-diabetic donors of 30 kPa and 50 kPa for LC samples from diabetic donors was measured. These differences were not statistically different either (Fig. 9C). Thus, according to our AFM measurements, DM and LC samples were of similar biomechanical properties (Fig. 9).

3. Discussion

We examined the proteomes of DMs and LCs by using a simplified LC-MS/MS method. Complemented with biomechanical measurements, these investigations showed that both BMs dramatically differ in protein compositions despite their similar morphological appearance. Further, the collagen IV-rich LC is mechanically weaker than the DM, which represents another surprising finding. While the proteomes of both BMs have been investigated previously (Ovodenko et al., 2007; Daylund et al., 2012; Poulsen et al., 2014; Uechi et al., 2014), this comparative approach of investigating the proteomes of both BMs side-by-side combined with biomechanical measurements revealed new aspects in the composition and biophysical properties these structures. While differences in protein compositions of both BMs were observed, the most remarkable finding was that the stoichiometry of collagen IV family members was consistently higher in the biomechanically softer LCs and low in the stiffer DMs. In addition, we found that TGFBIp, a protein that was previously not considered as a typical BM protein, has to be included as a significant component of human BMs.

3.1. Technical considerations

As previously shown, the composition of human BMs may change with age (Candiello et al., 2010). We therefore used for this study

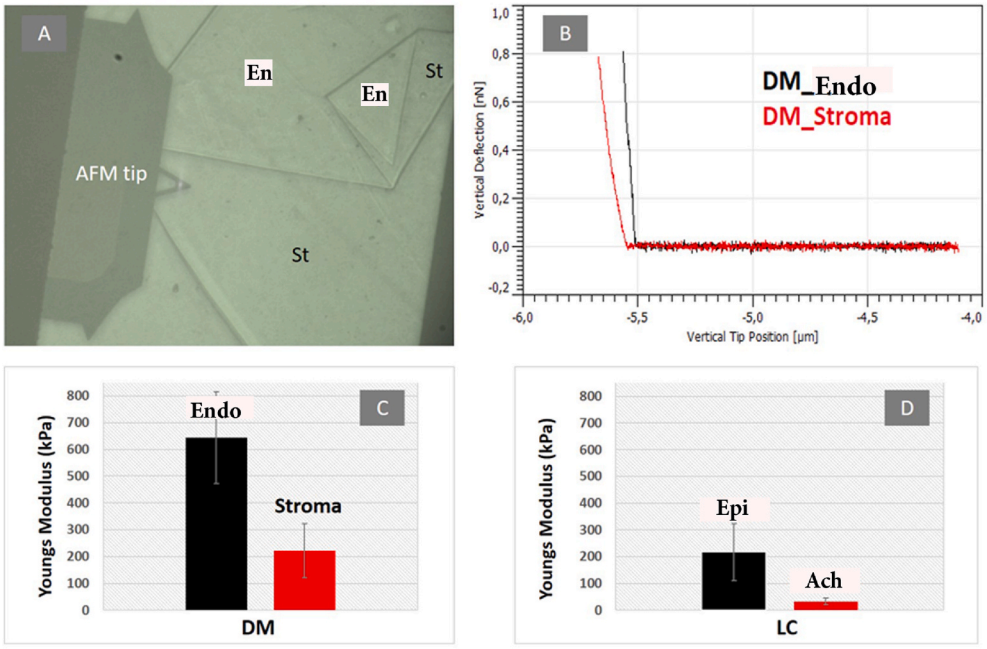

Fig. 8. Biomechanical testing of human DM and LC whole mounts by AFM. The image in panel (A) shows a light micrograph of a representative flat-mounted DM during the AFM measurements. The sample is multiply folded. En: endothelial side, St: stromal side. (B) Representative force measurements of the stromal and endothelial sides. The Bar graph in (C) contrasts the average stiffness of all measured DM samples from the endothelial (black) and from the stromal sides (red). The Bar graph in (D) contrasts the average stiffness of all measured LC samples from the epithelial (Epi; black) and from the anterior-chamber sides (Ach; red). In both cases, the endothelial/epithelial sides were stiffer than their respective stromal/anterior-chamber sides. (For interpretation of the references to colour in this figure legend, the reader is referred to the Web version of this article.)

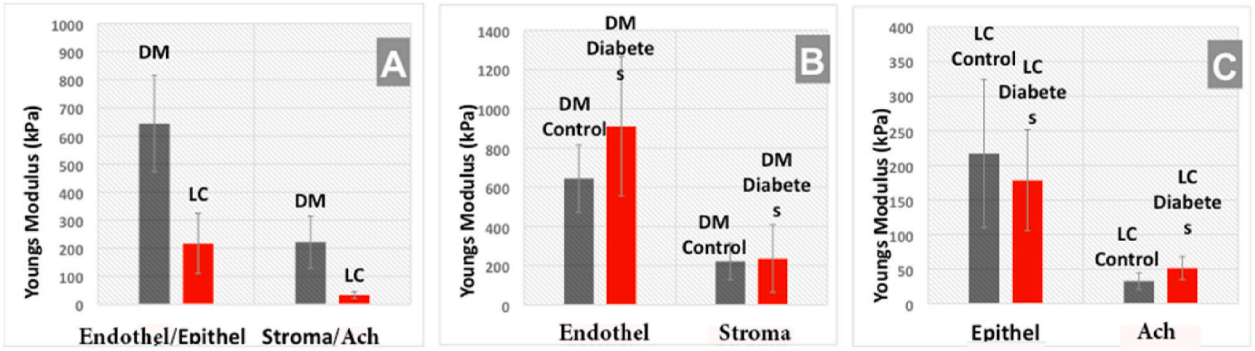

Fig. 9. Biomechanical testing of human DM and LC whole mounts (A). In panel A, the stiffness data from the endothelial/epithelial sides as well as the stromal/anterior-chamber sides of DM (grey) and LC (red) are compared side by side. The DM is much stiffer on both sides. Panel B and C compares the stiffness data of the DM and LCs from non-diabetic (grey) and diabetic (red) donors. The Bar graph in (B) contrasts the average stiffness of all measured DM samples from non-diabetic and diabetic patients at the endothelial (Endo) and the stromal sides. The Bar graph in (C) contrasts the average stiffness of all measured LC samples from non-diabetic (grey) and diabetic (red) patients at the epithelial (epithelial) and the anterior-chamber (Ach) sides. (For interpretation of the references to colour in this figure legend, the reader is referred to the Web version of this article.)

non-diabetic and diabetic samples from middle-aged donors ranging from 38 to 65 years of age. The sequential sample digestion with collagenase and trypsin led to a complete solubilization of the BMs and, thus, allowed a direct analysis of the released peptides by one-shot LC-MS/MS. This simplified sample preparation method has the advantage that neither excessively laborious and time-consuming pre-separation of BM proteins *via* SDS-PAGE nor a one-by-one analysis of the roughly twenty protein bands was required.

A recurrent problem in earlier analyses was that the protein quantity data did not always reflect the expected chain compositions of collagens and laminins (Ovodenko et al., 2007; Balasubramani et al., 2010; Dylund et al., 2012; Poulsen et al., 2014; Uechi et al., 2014). This was not the case in this study: we found that the LC exhibited an expected relative amount of collagen IVα1 that was close to double of that of collagen IVα2. Similar ratios were observed for ColIV α3, 4, 5, and 6. Likewise, the ratio of collagen VI to laminin α5, β1, β2 and γ1 was in a similar range. There was one unexpected case, in which in one of the DM samples collagen IVα1, but not any collagen IVα2, was detected. One possibility is that not all proteins fragmented as efficiently and thus remained undetected or under-represented. This is however unlikely for the present analysis, as the collagen IV α2 chain was readily detectable in the expected quantities of all six LC samples. It is also conceivable that the collagen members associate themselves into trimers that have previously not been considered to exist, or that the trimer-assembly of collagen IV is promiscuous and less strict than expected. In respect of detection and quantification of laminin and collagen IV family members, our analyses were more precise than previous publications, where laminin and collagen IV members were missed or detected in higher or lower concentrations as expected (Balasubramani et al., 2010; Ovodenko et al., 2007; Dylund et al., 2012; Poulsen et al., 2014; Uechi et al., 2014).

Another surprising observation was the absence of collagen VIII (Tamura et al., 1991; Hopfer et al., 2005) in all DM samples. Collagen VIII is considered a major component of the corneal stroma, and has previously been detected with up to 10% of all proteins in DM samples. These samples, however, included the adjacent endothelial cell layer and were not clean BM preparations. As a result, the typical BM proteins from the DMs accounted only to few percent of the entire proteome that was detected with these samples. As collagen VIII was undetectable in all of our LC-MS/MS analyses of the isolated, stroma- and endothelial-free DMs, we assume that collagen VIII is not tightly associated with the DM, and thus not an integral component which is lost during the detergent treatment (Tamura et al., 1991; Hopfer et al., 2005). In that context, it is worth noting that previous proteomic studies analyzed entire human corneas or DMs with their adherent endothelial cells (Dylund et al., 2012; Poulsen et al., 2014; Skele et al., 2018). In these cases, the BM proteins accounted for less than 5% of the detected proteins, while in our studies ECM proteins accounted on average for 60% of all detected proteins.

3.2. *Comparing the DM to the LC*

Consistent with earlier results (Ovodenko et al., 2007; Dylund et al., 2012; Poulsen et al., 2014; Uechi et al., 2014), the DMs and LCs included several collagen IV (Koshnoodi et al., 2008) and laminin family members (Hohenester and Yurchenco, 2013). Further components included nidogen 1, 2 and several proteoglycans, with keratokan, perlecan and agrin being the dominant family members (Iozzo, 2005).

But, the LC proteome also differed from that of the DM, the most evident difference being the relative concentrations of collagen IV family members (Khoshnoodi et al., 2008) These members accounted for approximately 70% of the total LC proteome, while collagen IV family members in the DM samples represented approximately 10% of the total DM proteome. While the presence of collagen IV family members has previously been recorded (Kelley et al., 2002), the immunocytochemical labeling did not allow any quantification and did not provide any data on the relative abundance of any of the collagen IV components.

Another variance was that the most abundant collagen IV type in the LC had a chain composition of α1α1α2, while that within the DM had a chain composition of α3α4α5. The LC also included a second major collagen IV trimer with a chain composition of α3α5α6. Thus, the two BMs differed in both their relative abundances as well in the trimer compositions of the collagen IV isoforms.

The laminin trimers (Hohenester and Yurchenco, 2013) were also different in both BMs, the LC variant consisting of LNα5β2γ1. This specific trimer is the most prominent type of laminin in human vascular BMs and inner limiting membranes. In the DM, the laminin trimer was composed of the α5, β1 and γ1 chains.

Yet another major difference was the abundance of TGF-beta1-induced protein (TGFBIp) in the DM, consistent with earlier studies (Skele et al., 2018). This 70kD-protein made up to 50% of the entire ECM proteome, while the protein was only sparsely detected in the LC. Mutations of this protein are responsible for several corneal dystrophies, mostly granular and lattice corneal dystrophies (Klinworth 2009). TGFBIp, also known as IG-H3, was first isolated from TGF-beta1-induced tumor cells (Skonier et al., 1992) and further identified in cartilage as an ECM protein that binds to native collagens, including collagen IV (Hashimoto et al., 1997). The binding to collagen IV even survived in the presence of 1M salt. TGFBIp is also abundant in corneal stroma, and its presence in DM may just be due to its abundant synthesis in the cornea

and its binding to collagen IV in BMs. While TGFBIp has not been considered a classical BM protein, proteome studies have now shown its presence in various BMs, (Randless et al., 2017), suggesting that it may have a generic, yet to be established, function in BM structure and function.

3.3. Biomechanical properties of the DM and LC

Probing the mounted DM and LC samples by force spectroscopy showed that the BM stiffness was in the high kPa range. Consistently, the endothelial/epithelial surface stiffness of the LC and DM was greater than that facing the stromal/anterior chamber layers. This bimodal distribution was consistent with prior AFM measurements of various ocular BMs (Halfter et al., 2013b), and supported by immunohistochemical analyses showing an abundance of laminin on the epithelial and an abundance of collagen IV α3 on the stromal sides (Fig. 7). An asymmetric organization of the DM has already been established with the detection of a striated and non-striated layer (Johnson et al., 1982).

The DM in our study is close to three times stiffer than the LC, a relationship that applies to both the epithelial and the stromal layers. In this context, an unexpected observation was that the collagen IV-rich LC was biomechanically softer than the DM despite its relatively small collagen IV content. The opposite was anticipated, as collagen IV is considered the protein providing BMs with mechanical stiffness (Yurchenco, 2011; Halfter et al., 2013b; Seikiguchi and Yamada, 2018). The current data therefore indicate that BM stiffness is not directly related to a high collagen IV concentration. While this does not dispute the importance of collagen IV in BM stiffness, it shows that collagen IV is not the only and most important factor in defining biomechanical stiffness. On the other hand, the higher stiffness of DM over LC makes sense, as a major function of the cornea and its DM represents a protective tissue of the eye, while the LC also has to provide elasticity and less stiffness for the ever-accommodating lens.

So far, a direct correlation of protein composition of both BMs and their stiffness could not be established. An aspect that has not been addressed but that may have a prominent role in BM stiffness is the crosslinking of BM proteins. Crosslinking may occur *via* the amino-terminal end of lysines/hydroxylysine with LOXL2 at the 7S domain, others *via* covalent sulfilimine-bonds between hydroxylysine and methionin in the NC1 domains (Cummings and Hudson, 2014) and finally *via* AGE, the advanced glycation end-products. A recent article showed that the corsslinks formed in collagen I fibrils in mouse tail tendons is formed from glycation end products. These crosslinks caused changes in the biomechanical properties of mouse tail tendon ECM, while other crosslinks did not (Stammers et al., 2020).

Previous studies using a hydrostatic device (Danielsen, 2004) and AFM (Ziebarth et al., 2011) investigated the biomechanical properties of human DMs and LCs. The data for LC by Ziebarth et al. (2011) showed Young's modulus of between 20 and 130 kPa for the LC, depending on the age of the donor. A distinction between the two sides was however not considered. We found Young's moduli of 200 kPa for the epithelial side and 30 kPa for the anterior chamber-side. The higher values in our study may account for the fact that Ziebarth et al. (2011) used trypsin and EDTA to remove the epithelial cells from the LC. Both reagents may digest and/or extract critical BM proteins, such as laminin, nidogen and other glycoproteins, from LC (Paulsson et al., 1986) and, thus potentially lower the stiffness the BM. The hydrostatic measurements by Danielsen (2004) found that LC and DM had similar Young's moduli of each 2.4 mPa, approximately 5- and 10-fold higher than our measurements. Again, a distinction of the two sides of the BM was not considered, and these hydrostatic measurements detected the mechanical stiffness of entire samples instead of specific BM surfaces. Previous AFM measurements (Last et al., 2009; Ali et al., 2016) of the endothelial side of the DM resulted in lower stiffness values than we observed (*i.e.,* 50 kPa). Again, the samples were obtained by EDTA treatment of the corneas, which may extract important BM proteins (Paulsson et al., 1986) and result in this lower stiffness.

3.4. The proteomes of DMs and LCs during diabetes

Previous studies have shown that the protein composition of vascular retinal BMs undergoes several changes with diabetes (Halfter et al., 2018). Consistently, the list of vascular BM proteins from diabetic eyes was by at least seven proteins longer, and several components of the complement system were detected in vascular BMs from diabetic eyes. Further, a variety of proteins were significantly more abundant in diabetic than in non-diabetic eyes. In contrast, our present analysis showed that the list of proteins in diabetic LCs and DMs exhibited only minor changes: The protein list from diabetic donor BMs was even shorter than that of non-diabetic DMs, which is opposite to the data obtained with vascular BMs. Few alterations were observed, but we were not able to associate any of these differences to a biological process, such as inflammation. In summary, the presented data strongly suggest that major changes in protein composition occur only in BMs that are in contact with elevated blood glucose levels. These apply prominently to vascular BMs, but are almost non-existent to non-vascular BMs, such as the LC and the DM. The same is true for the stiffness data: there was no statistically significant difference between diabetic and non-diabetic DMs and LCs. This was very much in difference to the vascular BMs, wiche were much softer after long-term diabetes.

Declaration of competing interest

The authors declare no competing interests.

Acknowledgments

The project was supported by an "Investigator-initiated, independent Research grant" from Bayer (Switzerland). We would also like to thank Drs. Nirmala SudarRaj, from the University of Pittsburgh for the J1 Mab to collagen IV α3.

Appendix A. Supplementary data

Supplementary data to this article can be found online at https://doi.org/10.1016/j.exer.2020.108326.

References

Ali, M., Raghunathan, V.K., Li, J.Y., Murphy, C.J., Thomasy, S.M., 2016. Biomechanical relationsships between the corneal endothelium and Descemet's membrane. Exp. Eye Res. 152, 57–70.
Balasubramani, M., Schreiber, E.M., Candiello, J., Balasubramani, G.K., Kurtz, J., Halfter, W., 2010. Molecular interactions in the retinal basement membrane system: a proteomics approach. Matrix Biol. 29, 471–483. PMID: 20403434.
Bruinsma, M., Tong, C.M., Melles, C.R., 2013. What does the future hold for the treatment of Fuchs endothelial dystrophy; will 'keratoplasty' still be a valid procedure? Eye 27, 1115–1122.
Candiello, J., Cole, G.J., Halfter, W., 2010. Age-dependent changes in the structure, composition and biophysical properties of a human basement membrane. Matrix Biol. 29, 402–410. PMID: 2036205.
Chen, J., Li, Z., Zhang, L., Ou, S., Wang, Y., et al., 2017. Descemet's membrane supports corneal endothelial regeneration in rabbits. Sci. Rep. 7, 6983.
Costell, M., Gustafsson, E., Aszodi, A., Moergelin, M., Bloch, W., Hunziger, E., Addicks, K., Timpl, R., Faessler, R., 1999. Perlecan maintains the integrity of cartilage and some basement membranes. J. Cell Biol. 147, 1109–1122. PMID: 10579729.
Cummings, C.F., Hudson, B.G., 2014. Lens capsule as a model to study type IV collagen. Connect. Tissue Res. 55, 8–12.
Danielsen, 2004. Tensile mechanical and creep properties of Descemet's membrane and lens capsule. Exp. Eye Res. 79, 343–350.
Danysh, B.P., Dunken, M.K., 2009. The lens capsule. Exp. Eye Res. 88, 151–164.
de Oliveira, R.C., Wilson, S.E., 2020. Descemet's membrane development, structure, function and regeneration. Exp. Eye Res. 197, 108090.
Droisum, L., Haaskjold, E., Sandwig, K., 1998. Phcoemulsification in eyes with pseudoexfoliation syndrom. J. Cataract Refract. Surg. 24, 787–792.
Dylund, T.F., Poulsen, E.T., Scavenius, C., Nikolajen, C.L., Thorgersen, I.B., Vorum, H., Enghild, J.J., 2012. Human cornea proteome: identification and quantification of the

proteins of the three main layers, including epithelium, stroma, and endothelium. J. Proteome Res. 11, 4231–4239.
Erickson, A.C., Couchman, J.R., 2000. Still more complexity in mammalian basement membranes. J. Histochem. Cytochem. 48, 1291–1306. PMID: 10990484.
Hafter, W., Moes, S., Asgeirsson, D.O., Oertle, P., Melo-Herraiz, E., Plodinec, M., Jenoe, P., Henrich, P.B., 2018. Diabetes-related changes in the protein composition and biomechanical properties of human retinal vascular basement membranes. PloS One 12, e0189857.
Halfter, W., Candiello, J., Hu, H., Zhang, P., Schreiber, E., Balasubramani, M., 2013a. Protein composition and biomechanical properties of in vivo-derived basement membranes. Cell Adhes. Migrat. 7, 64–71.
Halfter, W., Monnier, C., Loparic, M., Uechi, G., Balasubramani, M., Henrich, P.B., 2013b. The bi-functional organization of human basement membranes. PloS One 8, e67660. PMID: 23844050.
Halfter, W., Oertle, P., Monnier, C.A., Camenzind, L., Reyes-Lua, M., Hu, H., Candiello, J., Labilloy, A., Balasubramani, M., Henrich, P.B., Plodinec, M., 2015. New concepts in basement membrane biology. FEBS J. 282, 4466–4479.
Hashimoto, K., Noshiro, M., Ohno, S., Kawamoto, T., Salakeda, H., Akagawa, Y., Nakashima, K., Okimura, A., Ishida, H., okamoto, T., Pan, H., Shen, M., Yan, W., Kato, Y., 1997. Characterization of a cartilage-derived 66-kD protein (RGD-CAP/big-H3) that binds to collagen. BBA 1355, 303–314.
Hohenester, E., Yurchenco, P.D., 2013. Laminins in basement membrane assembly. Cell Adhes. Migrat. 7, 56–63.
Hopfer, U., Fukai, N., Hopfer, H., et al., 2005. Targeted disruption of Col18a2 in mice leads to anterior segment abnormalities in the eye. Faseb. J. 19, 1232–1244.
Iozzo, R.V., 2005. Basement membrane proteoglycans: from cellar to ceiling. Nat. Rev. Mol. Cell Biol. 6, 646–656.
Janmey, P.A., McCulloch, C.A., 2007. Cell mechanics: integrating cell response to mechanical stimuli. Annu. Rev. Biomed. Eng. 9, 1–34.
Johnson, D.H., Bourne, W.M., Campbell, R.J., 1982. The ultrastructure of Descemet's membrane. I. Changes with age in normal corneas. Arch. Ophthalmol. 100, 1942–1947.
Kelley, P.B., Sado, Y., Duncan, M.K., 2002. Collagen IV in the developjng lens capsule. Matrix Biol. 211, 415–423.
Khoshnoodi, J., Pedchenco, V., Hudson, B.G., 2008. Mammalian collagen IV. Microsc. Res. Tech. 71, 3578-370.
Klintworth, G.K., et al., 2009. Corneal dystrophies. Orphanet J. Rare Dis. 4, 7–45.
Kobasova, A., Azar, D.T., Bannikov, G.A., Campbell, K., Durbeej, M., Ghohesiani, et al., 2007. Composititonal differences between infant and adult human corneal basement membranes. Invest. Ophthalmol. Vis. Sci. 48, 4869–4899.
Last, J.A., Liliensieck, S.J., Murphy, C.J., 2009. Determining the mechanical properties of human corneal basement membranes with atomic force microscopy. J. Struct. Biol. 167, 19–24.
Loukovitis, E.C., Kozeis, N., Gatzioufas, Z., Kozei, A., Tsotridou, E., Stoila, M., Koronis, S., Sfakianakis, K., Tranos, P., Balidis, M., Zachariadis, Z., Mikropoulos, D.G., Anogeianakis, G., Katsanos, A., Konstas, A.G., 2019. The proteins of keratoconus: a literature review exploring their contribution to the pathophysiology of the disease. Adv. Ther. 36, 2205–2222.
Minamide, L.S., Bamberg, J.R., 1990. A filter paper dye-binding assay for quantitative determination of protein withput interference from reducing agents or detergent. Anal. Biochem. 190, 66–70.
Miner, J.H., Cunningham, J., Sanes, J.R., 1998. Roles of laminin in embryogenesis: exencephaly, syndactyly, and placentopathy in mice lacking the laminin alpha5 chain. J. Cell Biol. 143, 1713–1723. PMID: 9852162.
Neilson, K.A., Ali, N.A., Muralidharan, S., Mirzaei, M., Mariani, M., Assadourian, G., Sluyter, S.C., Haynes, P.A., 2011. Less label, more free: approaches in label-free quantitative mass spectrometry. Proteomics 11, 535–553.
Oliver, W.C., Pharr, G.M., 1992. An imroved technique for determining hardness and elastic modulus using load and displacement sensing indentation experiments. J. Mater. Res. 7, 1564–1583.
Ovodenko, B., Rostagno, A., Neubert, T.A., Shetty, V., Thomas, S., Yang, A., Liebmann, J., Gbiso, J., Rich, R., 2007. Proteome analysis of exfoliation syndrome. Invest. Ophthalmol. Vis. Sci. 48, 1447–1457.
Pandey, N., John, S., 2020. Keyser-fleischer ring. Aug 11. In: StatPearls [Internet]. Treasure Island (FL): StatPearls Publishing. PMID: 29083643.
Paulsson, M., Aumailley, R., Timpl, R., Keck, K., Engel, J., 1986. Laminin-nidogen-complex. Extraction with chelating agents and structural characterization. Eur. J. Biochem. 166, 11–19.
Pöschl, E., Schlotzer-Schrenhardt, U., Brachvogel, B., Saito, K., Ninomiya, Y., Mayer, U., 2004. Collagen IV is essential for basement membrane stability but dispensable for initiation of its assembly during early development. Development 131, 1619–1628. PMID: 14998921.
Poulsen, E.T., Dyrlund, T.F., Runager, K., Scavenius, C., Krogager, T.P., Hojrup, P., Thorgersen, I.B., Sangaard, K.W., Vorum, H., Hjortdal, J., Enghild, J.J., 2014. Proteomics of Fuchs endothelial dystrophy support that the extracellular matrix of Descement's membrane is disordered. J. Proteome Res. 13, 4639–4667.
Randless, M.J., Humphries, M.J., Lennon, R., 2017. Proteomic definitions of basement membrane composition in health and disease. Matrix Biol. 57, 12–28.
Reyes-Lua, M., Oertle, P., Camenzind, L., Goz, A., Meyer, C.H., Konieczka, K., Loparic, M., Halfter, W., Henrich, P.B., 2016. Superior rim stability of the lens capsule following manual over fentoseond laser capsulotomy. Invest. Ophthalmol. Vis. Sci. 57, 2839–2847.
Robitaille, A.M., Christen, S., Shimobayashi, M., Cornu, M., Fava, L.L., Moes, S., Prescianotto-Baschong, C., Sauer, U., Jenoe, P., Hall, M.N., 2013. Quantitative phosphoproteomics reveal mTORC1 activates de Novo pyrimidine synthesis. Science 339, 1320–1323.
Sader, J.E., Chon, W.M., Mulvaney, P., 1999. Calibration of rectangular atomic force microscope cantilevers. Rev. Sci. Instrum. 70, 3967–3969.
Seikiguchi, K., Yamada, K.M., 2018. Basement membranes in development and disease. Curr. Top. Dev. Biol. 130, 143–191.
Skele, J.M., Aldrich, B.T., Goldstein, A.S., Schmidt, G.A., Reed, C.R., Greiner, M.A., 2018. Proteomic analysis of corneal endotelial cell-descemet membrane tissue reveals influence of insulin-dependence and disease severity in type 2 diabetes mellitus. PloS One 12, e0192287.
Skonier, J., Neubauer, M., Madisen, L., Bennett, K., Plowman, G.D., Purchio, A.F., 1992. cDNA cloning and sequence analysis of beta Ig-H3, a novel gene induced in a adenocarcinoma cell line after treatment with transforming growth factor beta. DNA Cell Biol. 11, 511–522.
Smyth, N., Vatansever, N.S., Murray, P., Meyer, M., Frie, C., Paulsson, M., Edgar, D., 1999. Absence of basement membranes after targeting the LANC1 gene results in embryonic lethality due to failure of endoderm differentiation. J. Cell Biol. 144, 151–160. PMID: 9885251.
Stammers, M., Ivanova, I.M., Niewczas, I.S., Segonds-Pichon, A., Streeter, M., Spiegel, D. A., Clark, J., 2020. Age-related changes in the physical properties, crosslinking, and glycation of collagen from mouse tail tenson. J. Biol. Chem. 295, 10562–10571.
Sundarraj, N., Wilson, J., 1982. Monoclonal antibody to human basement membrane collagen type IV. Immunology 47, 133–140. PMID: 6811420.
Tamura, Y., Konomi, H., Sawada, H., et al., 1991. Tissue distribution of type VIII collagen in human adult and fetal eyes. Invest. Ophthalmol. Vis. Sci. 32, 2636–2644.
Timpl, R., Brown, J.C., 1996. Supramolecular assembly of basement membranes. Bioassays 18, 123–132. PMID: 8851045.
To, M., Candiello, J., Sullivan, M., Farhad Safi, F., Andrew Eller, A., Halfter, W., 2013. Diabetes-induced morphological and compositional changes in ocular basement membranes. Exp. Eye Res. 16, 298–307. PMID: 24095823.
Uechi, G., Sun, Z., Schreiber, E.M., Halfter, W., Balasubramani, M., 2014. Proteomic view of basement membranes from human retinal blood vessels, inner limiting membranes, and lens capsules. J. Proteome Res. 13, 3693–3705. PMID: 24990792.
Wilson, M.R., Easterbrook-Smith, S.B., 2000. Clusterin is a secreted mammalian chaperone. Trends Biochem. Sci. 25, 95–98.
Wisniewski, J.R., Zougman, A., Nagaraj, N., Mann, A., 2009. Universal sample preparation method for proteome analysis. Nat. Methods 6, 359–362.
Wyatt, A., Yerbury, J., Poon, S., Dabbs, R., Wilson, M., 2009. The chaperone action of clusterin and its putative role in quality control of extracellular matrix folding. Adv. Canc. Res. 104, 89–111.
Yurchenco, P.D., 2011. Basement membranes; Cell scaffolds and signaling platforms. Cold Spring Harb. Perspect. Biol. 3a, 004911.
Zhang, D.J., Patel, D.V., 2015. The pathophysiology of Fuchs' endothelial dystrophy–a review of molecular and cellular insights. Exp. Eye Res. 130, 97–105.
Zhang, W., Kassels, A.C., Barrington, A., Khan, S., Tomatsu, S., Alkadi, T., Aldave, A., 2018. Macular corneal dystrophy with isolated peripheral Descemets membrane deposits. Am. J. Ophthalmol. Case Rep. 16, 100571.
Ziebarth, N.M., Arrieta, E., Feuer, W.J., Moy, V.T., Mann, S.F., Parel, J.M., 2011. Primate lens capsule elasticity assessed by Atomic Force Microscopy. Exp. Eye Res. 92, 490–494.